Biosensors and Bioelectronics 52 (2014) 153–158

Contents lists available at ScienceDirect

Biosensors and Bioelectronics

journal homepage: www.elsevier.com/locate/bios

Nanogold/mesoporous carbon foam-mediated silver enhancement for graphene-enhanced electrochemical immunosensing of carcinoembryonic antigen

Dajie Lin [a,1], Jie Wu [a,1], Huangxian Ju [a,*], Feng Yan [b,*]

[a] State Key Laboratory of Analytical Chemistry for Life Science, Department of Chemistry, Nanjing University, Nanjing 210093, PR China
[b] Jiangsu Institute of Cancer Prevention and Cure, Nanjing 210009, PR China

ARTICLE INFO

Article history:
Received 27 June 2013
Received in revised form
13 August 2013
Accepted 22 August 2013
Available online 31 August 2013

Keywords:
Electrochemical sensors
Immunoassay
Signal amplification
Silver deposition
Mesoporous carbon foam
Graphene

ABSTRACT

Nanogold functionalized mesoporous carbon foam (Au/MCF) coupling with a signal amplification by C–Au synergistic silver enhancement was designed for sensitive electrochemical immunosensing of biomarker. The Au/MCF was prepared by in situ growth of nanogold on carboxylated MCF and used as a tracing tag to label signal antibody via the inherent interaction between protein and nanogold. The immunosensor was prepared by covalently immobilizing capture antibody on an electrochemically reduced graphene oxide/chitosan film modified glassy carbon electrode. Through a sandwich-type immunoreaction, Au/MCF tags were captured on the immunoconjugates to induce a silver deposition process. The electrochemical stripping signal of the deposited silver was used to monitor the immunoreaction. The Au/MCF-mediated silver enhancement along with the graphene-promoted electron transfer led to high detection sensitivity of carcinoembryonic antigen. Under optimal conditions, the proposed immunoassay method showed wide linear range from 0.05 pg mL^{-1} to 1 ng mL^{-1} and a detection limit down to 0.024 pg mL^{-1}. The newly designed amplification strategy holds great potential for ultrasensitive electrochemical biosensing of other analytes.

1. Introduction

The levels of tumor markers in blood or tissue provide essential information for clinical cancer screening and disease diagnosis (Sidransky, 2002; Wulfkuhle et al., 2003). Carcinoembryonic antigen (CEA), one of the most extensively used tumor marker, is expressed in many malignancies, such as lung cancer, ovarian carcinoma, breast cancer, and cystadenocarcinoma (Kong et al., 2011). Therefore, the sensitive determination of CEA is very important in clinical research and early diagnosis. Among various immunoassay methods, electrochemical immunosensing has been well developed due to its intrinsic advantages of good portability, low cost, and high detection sensitivity (Nie et al., 2009; Malhotra et al., 2010; Lin et al., 2013). With the development of nanoscience and nanotechnology, various types of nanomaterials have been applied to amplify the electrochemical response and construct the ultrasensitive biosensors. Most of the signal amplification strategies are performed by conjugating large amounts of signal or signal-related molecules, such as enzymes (Wang et al., 2004; Wu et al., 2009; Zhuo et al., 2009; Malhotra et al., 2010), quantum dots (Tang et al., 2013; Wu et al., 2013), and metal nanoparticles (Ho et al., 2010; Lai et al., 2011; Lin et al., 2012), on various nanocarriers, such as carbon nanotubes (CNTs) (Wang et al., 2004; Lai et al., 2011), magnetic beads (Zhuo et al., 2009; Malhotra et al., 2010), and nanoparticles (Wu et al., 2009, 2013), to trace the immunoreactions.

Due to the good biocompatibility and easy functionalization with biomolecules, gold nanoparticles (AuNPs) have been extensively applied as a favorable nanocarrier of signal molecules in immunoassays (Katz and Willner, 2004; Malhotra et al., 2010; Liu et al., 2011). Furthermore, AuNPs can be used as attractive electroactive labels for design of enzyme-free immunosensing strategies by electrochemical stripping analysis (Dequaire et al., 2000). Compared with the relatively positive electrochemical oxidization potential of AuNPs, silver nanoparticles (AgNPs) can be more easily oxidized for stripping analysis with a relatively sharp peak (Ting et al., 2009). Thus AuNPs-mediated silver enhancement after specific recognition with analytes has been proposed for sensitive electrochemical detection of DNA (Taton et al., 2000) and immunoassay of proteins (Kim et al., 2009; Lin et al., 2012).

Recently, carbon materials, such as graphene and carbon nanotubes, have been reported to process favorable features

* Corresponding authors. Tel./fax: +86 25 83593593.
E-mail addresses: hxju@nju.edu.cn (H. Ju), yanfeng2007@sohu.com (F. Yan).
[1] These authors contributed equally to this work.

0956-5663/$ - see front matter © 2013 Elsevier B.V. All rights reserved.
http://dx.doi.org/10.1016/j.bios.2013.08.051

catalyzing the silver deposition (Lai et al., 2011; Qu et al., 2011; Wan et al., 2011). Mesoporous carbon has also gained great interest for the application in biosensing (Walcarius, 2012) due to its good biocompatibility, high electrical conductivity, nice chemical and mechanical stability, extensive large surface area, well-ordered pore structure, and special surface reactivity (Boo et al., 2005; Wu et al., 2007; Deng et al., 2010; Wang et al., 2010; Lu et al., 2012). It even shows superior performance than carbon nanotubes in electrochemical biosensing (Zhou et al., 2008). Thus this work combined the advantages of AuNPs and mesoporous carbon foam (MCF) to design a synergistic Au/MCF-mediated silver enhancement process by in situ growth of nanogold on carboxylated MCF. This signal amplification process could be conveniently applied in sensitive immunosensing of biomarker using a graphene-enhanced electrochemical immunosensor.

Graphene, a single layer of carbon atoms with a closely packed honeycomb in a two-dimensional lattice, has become a common matrix for construction of electrochemical sensing platform due to its fast electron transportation (Wang et al., 2010; Lin et al., 2012). This work used chitosan film to immobilize graphene oxide on a glassy carbon electrode (GCE) and then in situ electrochemically reduced the graphene oxide for the preparation of immunosensor. Chitosan acted as a biocompatible membrane material for covalent binding of capture antibody. The graphene-promoted electron transfer could remarkably increase the sensitivity of the biosensor. The present assay approach showed a detection limit down to 0.024 $pgmL^{-1}$ for CEA, which was lower than those using nanomaterial-based multi-enzyme amplification strategies (Malhotra et al., 2010; Tang et al., 2011).

2. Material and methods

2.1. Material and reagents

Mouse monoclonal capture (Ab_1) and signal (Ab_2) anti-CEA antibodies (clone no. 27D6 and 28E4) were purchased from Shuangliu Zhenglong Biochem. Lab (Chengdu, China). Silver enhancer solutions A and B, and chitosan were purchased from Sigma-Aldrich (USA). Bovine serum albumin (BSA) was obtained from Nanjing SunShine Biotechnology Co., LTD. (China). CEA standard solutions were from CEA ELISA kit, which was supplied by Fujirebio Diagnostics AB (Göteborg, Sweden). Chloroauric acid ($HAuCl_4 \cdot 4H_2O$) was obtained from Shanghai Reagent Company (Shanghai, China). Ultrapure water obtained from a Millipore water purification system (≥ 18 MΩ, Milli-Q, Millipore) was used in all assays. The clinical serum samples were from Jiangsu Institute of Cancer Research. All other reagents were of analytical grade and used as received.

Tris–HNO_3 buffer (0.1 M, pH 7.4) containing 0.05% (w/v) Tween-20 was used as the washing solution. 0.1 M Tris–HNO_3 containing 5% BSA was used as blocking solution for the preparation of immunosensor. The mixture of silver enhancer solutions A and B was freshly diluted at 20 times for silver deposition.

2.2. Apparatus

The morphologies of the MCF and Au/MCF were examined using a JEM 2100 high-resolution transmission electron microscope (TEM) (Japan). X-ray photoelectron spectroscopy (XPS) measurements were performed using a PHI5000 Versa Probe spectrometer (ULVAC-PHI, Japan). Nitrogen adsorption–desorption isotherms and pore size distributions were measured at 77 K using a Micrometeritics ASAP 2020 system. All electrochemical immunoassays were performed on a CHI 660D electrochemical workstation (Chenhua, Shanghai, China). The reference levels of CEA in the human serum samples were detected with an automation electrochemiluminescent analyzer (Elecsys 2010, Roche).

2.3. Preparation of Ab_2 functionalized Au/MCF

The MCF was synthesized according to the previous report (Tao et al., 2013). MCF (40 mg) were dispersed in 60 mL of 30% HNO_3 and then refluxed for 24 h at 140 °C to obtain carboxylic group functionalized MCF. The carboxylated MCF was washed repeatedly with water until the pH reached 7.0.

As shown in Scheme 1A, the Au/MCF was prepared according to the previous report with minor modification (Datta et al., 2010). Typically, 0.5 mL of 25 mM $HAuCl_4$ was added to 40 mL 0.25 mg mL^{-1} MCF under mild sonication for 30 min, followed by dropwise addition

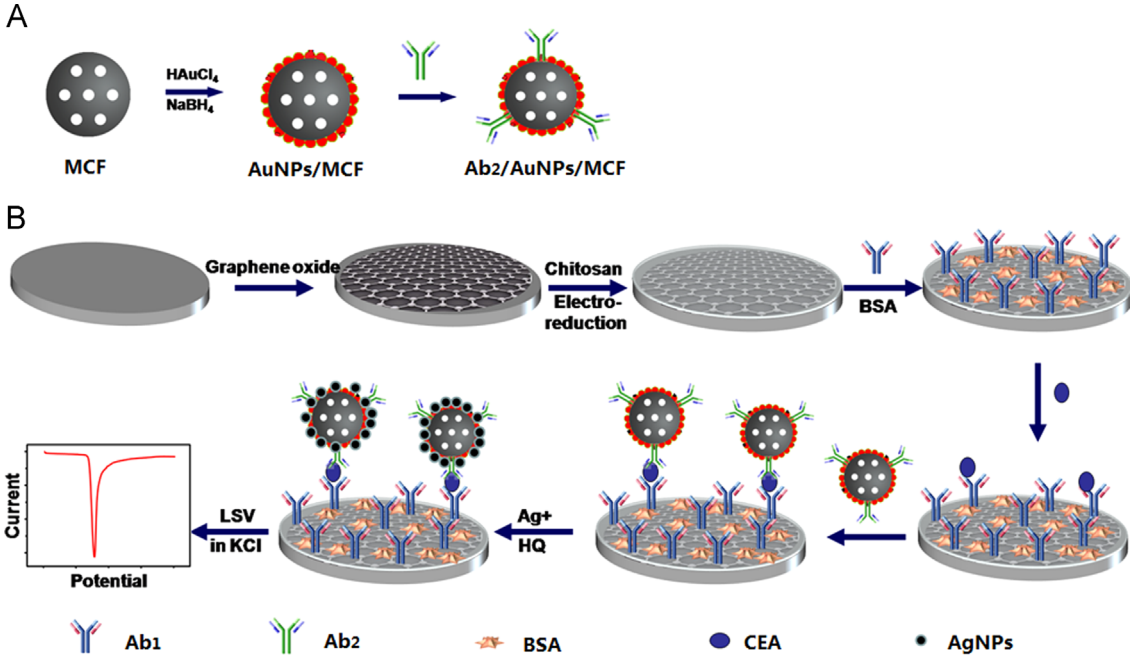

Scheme 1. Schematic representation of (A) the preparation of Ab_2/Au/MCF, and (B) the immunosensor fabrication and sandwich-type immunoassay procedure.

of 1 mL freshly prepared ice-cold $NaBH_4$ (0.1 M). After stirring for 20 min, the Au/MCF formed was isolated by centrifugation (9000 rpm), dispersed in 20 mL water and stored at 4 °C.

15 μL of 20 μg mL^{-1} Ab_2 was added into 1 mL of Au/MCF suspension, which was previously adjusted to pH 9.2, followed by incubation at 4 °C for 4 h with slow stirring. Afterwards, the suspension was incubated with 0.1 mL of blocking buffer with gently stirring at 4 °C for 2 h. Then, the product was centrifuged at 9000 rpm for 15 min. After twice washing with pH 7.4 Tris–HNO_3, the obtained Ab_2 functionalized Au/MCF (Ab_2/Au/MCF) was dispersed in 1 mL of pH 7.4 Tris–HNO_3 containing 0.1% BSA.

2.4. Fabrication of immunosensor

The GCE with 3-mm diameter was polished to a mirror using 1.0, 0.3 and 0.05 μm alumina slurry (Buehler) followed by rinsing thoroughly with deionized water. After successive sonication in 1:1 nitric acid, acetone and deionized water, the electrode was rinsed with water and allowed to dry at room temperature. 5 μL of 0.5 mg mL^{-1} graphene solution, which was synthesized from graphite by the Hummers method (Darbha et al., 2008), was then dropped on the pretreated GCE and was dried in air (Scheme 1B). After 3 μL of 0.05% chitosan solution was dropped on the graphene film and dried in air, the electrochemical reduction of graphene oxide was performed at −1.0 V in pH 8.0 PBS, and the modified electrode was washed with water and incubated with 5 μL of 2.5% glutaraldehyde (in 50 mM PBS, pH 7.4) for 2 h. After the electrode was further washed with water, 5 μL of 0.2 mg mL^{-1} Ab_1 was dropped onto its surface to incubate at room temperature for 60 min and 4 °C overnight in a 100% moisture-saturated environment. Subsequently, excess antibody was removed with washing buffer and pH 7.4 Tris–HNO_3, respectively. Finally, 5 μL of blocking solution was dropped on the electrode surface and incubated for 60 min at room temperature to block possible remaining active sites against nonspecific adsorption. After another wash with washing buffer and pH 7.4 Tris–HNO_3, the immunosensor was obtained.

2.5. Immunoassay procedure

To carry out the immunoassay, the immunosensor was firstly incubated with 5 μL of CEA standard solution or serum sample with certain concentration for 40 min at 37 °C (Scheme 1B). After washed with washing buffer and pH 7.4 Tris–HNO_3, the immunosensor was further incubated with 5 μL of Ab_2/Au/MCF for 40 min at 37 °C. Upon another washing process, silver-deposition enhancement was performed by adding 10 μL mixture of enhancer solutions on the immunosensor surface and incubating for 4 min at 37 °C, which was protected from light. The immunosensor was finally rinsed with water to carry out the anodic stripping analysis from −0.08 to 0.2 V at 50 mVs^{-1} in 1.0 M KCl solution.

3. Results and discussion

3.1. Characterization of Ab_2/Au/MCF

The detection property of the probe was related to the nanostructure of MCF. For example, the bigger size of MCF could produce a greater amplification, hence, a lower detection limit, while it provided a relatively narrow linear detection range due to the steric effect. In addition, the size of pores in MCF influenced the growth of AuNPs. Narrow pores were found to enhance the stability of metal particles due to the partial confinement of these particles by the pore walls (Prieto et al., 2013). Thus, the nanostructure of MCF was firstly characterized in detail. The TEM image of MCF showed uniformly distributed mesostructured cells (Fig. 1A), indicating the successful synthesis of MCF with an ordered mesocellular structure. The N_2 adsorption–desorption isotherms of MCF exhibited a typical mesopore hysteresis loop with adsorption and desorption branches at high relative pressures (Fig. 1B), indicating the type IV structure with IUPAC classification (Tao et al., 2013). The surface area of MCF determined by Brunanuer–Emmer–Teller (BET) test was as high as 516 m^2 g^{-1}, and the pore size distribution curve exhibited a diameter of 4 nm (Fig. 1C). After the in situ growth of nanogold, numerous "Au

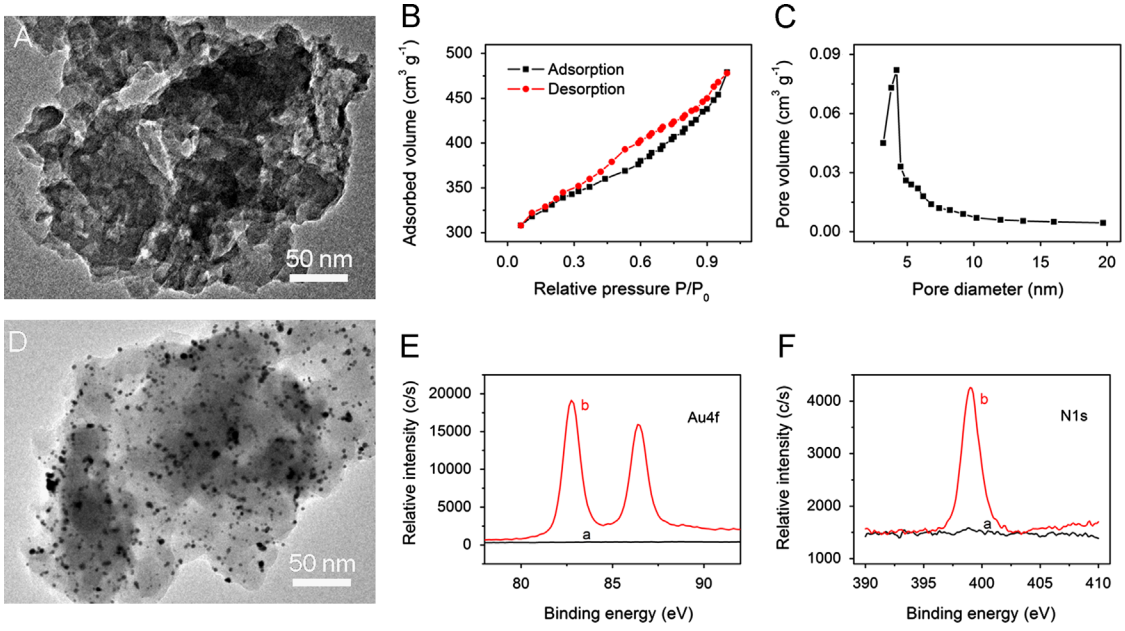

Fig. 1. (A) TEM image, (B) nitrogen adsorption–desorption isotherms and (C) pore size distribution of the MCF; (D) TEM image of the Au/MCF; (E) XPS spectra of the MCF (a) and Au/MCF (b); (F) XPS spectra of Au/MCF (a) and Ab_2/Au/MCF (b).

islands" were observed on the surface of MCF with homogenous and individual distribution (Fig. 1D). Contrast to the XPS spectrum of MCF, obvious Au4f peaks at 82.77 and 86.43 eV were observed on the XPS spectrum of Au/MCF (Fig. 1E).

Through the interaction between AuNPs and the mercapto or amino group of protein, the Au/MCF could easily be labeled to the secondary antibody to form Ab_2/Au/MCF. The XPS spectrum of Ab_2/Au/MCF showed an obvious N1s peak at 399.0 eV, which was from the amino group of antibody, while no N1s peak was observed in the XPS spectrum of Au/MCF (Fig. 1F). This result confirmed the successful modification of Ab_2 on Au/MCF.

3.2. Characterization of immunosensor and signal amplification

Graphene, especially electrochemically reduced graphene, has been widely used in constructing immunosensor to improve the detection sensitivity due to its high conductivity to mediate the electron transfer (Lin et al., 2012). This work used electrochemically reduced graphene oxide film to construct the immunosensor. The change in interfacial properties was monitored with electrochemical impedance spectroscopy (EIS) with a redox couple of $[Fe(CN)_6]^{3-/4-}$. The chitosan/GCE showed an electron-transfer resistance, R_{et}, of 402 Ω, while the R_{et} at chitosan/graphene oxide/GCE was 198 Ω (Fig. 2A), implying that graphene is an excellent electric conducting material to accelerate the electron transfer. After electrochemical reduction of the graphene oxide, the R_{et} further decreased, indicating the reduced graphene could more efficiently accelerate the electron transfer for producing higher sensitivity.

After sandwich-type immunoreaction, the Ab_2/Au/MCF was captured on the surface of the immunosensor by the formation of immunocomplex. With further incubation with silver enhancer solutions, the AgNPs could be induced to deposit on the surface of the immunosensor, which could be easily detected by anodic stripping voltammetric analysis with a sharp stripping peak in the presence of Cl^- (Fig. 2B). The peak current increased with the increasing concentration of antigen used in the sandwich immunoreaction, and could thus be used for immunoassay. When using the signal antibody Ab_2 and 0.1 ng mL^{-1} CEA for sandwich-type immunoreactions, the silver deposition led to a stripping voltammetric response of 12.7 μA (curve a, Fig. 2B). This response resulted from the chemical reduction of Ag^+ in the absence of the catalysis, Au/MCF, thus could be thought as a background signal of this method. After using Ab_2/MCF to replace Ab_2 for the immunoreactions, the silver deposition produced a higher stripping peak current of 32.8 μA (curve b, Fig. 2B), indicating MCF could catalyze the silver deposition to produce more AgNPs on the immunosensor surface. The catalytic property of MCF was attributed to the plentiful surface carboxyl groups, which could act as anchor sites for in situ silver deposition (Li et al., 2007; Qu et al., 2011). With the same conditions Ab_2/Au/MCF probe produced a response of 64.2 μA (curve c, Fig. 2B), which was about two times higher than that of Ab_2/MCF, indicating a C–Au synergistic silver enhancement.

3.3. Optimization of detection conditions

As the amount of reduced graphene was related to the amount of graphene oxide modified on the sensor, the effect of graphene oxide concentration on immunosensor response towards 0.1 ng mL^{-1} CEA was investigated (Fig. S1). With the increasing concentration of graphene from 0 to 1.0 mg mL^{-1}, the current response increased first to the maximum at 0.5 mg mL^{-1} and then decreased. This was due to the increasing graphene oxide amount, which produced more reduced graphene to improve the electron transfer. However, higher concentration of graphene would cause aggregation, resulting in the decrease of the current response. Thus, 0.5 mg mL^{-1} graphene oxide was optimized to prepare the immunosensor.

The amount of deposited silver at the immunosensor surface increased with the increasing concentration of silver enhancer solutions. However, higher concentrations of silver enhancer solutions produced higher background current. So this work used the signal to noise ratio (S/N) to optimize the deposition conditions. Upon the successive dilution of silver enhancer solutions, the S/N quickly increased and trended to a maximum value at 20-fold dilution (Fig. 3A). Thus the enhancer solutions with 20-fold dilution were used for silver deposition.

The incubation time is another important parameter affecting the analytical performance of immunoassay. With the increasing incubation time, the stripping peak current for CEA increased and trended to a constant value after an incubation time of 40 min (Fig. 3B), which showed a saturated binding between the analyte and the capture antibody. Therefore, the incubation time of 40 min was selected for the sandwich-type immunoassay.

3.4. Analytical performance

Under the optimum conditions, the stripping peak current of AgNPs deposited on the immunosensor increased with increasing concentration of CEA in the incubation solution (Fig. 4A). The calibration plot showed a good linear relationship between the stripping peak current and the logarithm of analyte concentration in the range from 0.05 pg mL^{-1} to 1.0 ng mL^{-1} with a correlation coefficient of 0.9997 (Fig. 4B). The limit of detection at a S/N of 3σ (where σ is the standard deviation of signal in a blank solution) was 0.024 pg mL^{-1}, which was much lower than those reported previously using nanomaterial-based multi-enzyme amplification strategies (Malhotra et al., 2010; Du et al., 2011; Tang et al., 2011) and AuNPs/microbeads

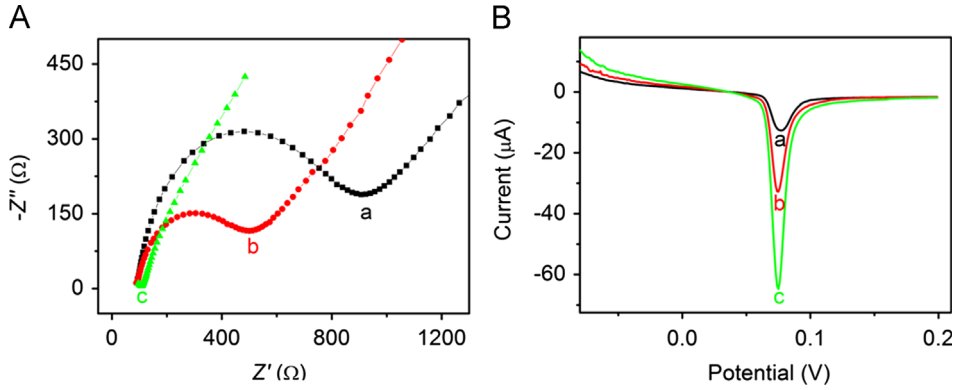

Fig. 2. (A) EIS of chitosan/GCE (a), chitosan/grapheme oxide/GCE (b), and chitosan/electrochemically reduced grapheme oxide/GCE (c) in 0.1 M KCl containing 5 mM $[Fe(CN)_6]^{3-/4-}$; (B) Stripping voltammetric responses of the immunosensor in 1.0 M KCl after sandwich immunoreactions with 0.1 ng mL^{-1} CEA and Ab_2 (a), Ab_2/MCF (b), and Ab_2/Au/MCF (c).

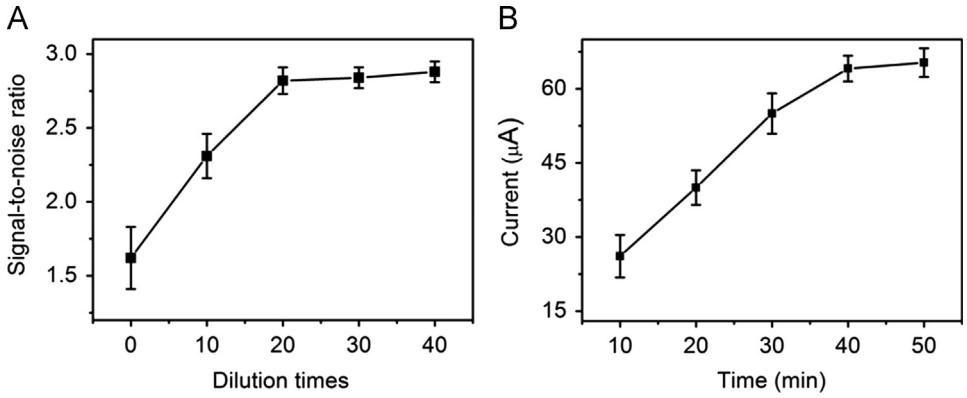

Fig. 3. (A) Ratios of signal to noise at different dilutions of silver enhancer solutions, and (B) dependence of stripping peak current on incubation time at 0.1 ng mL^{-1} CEA ($n=3$ for error bars).

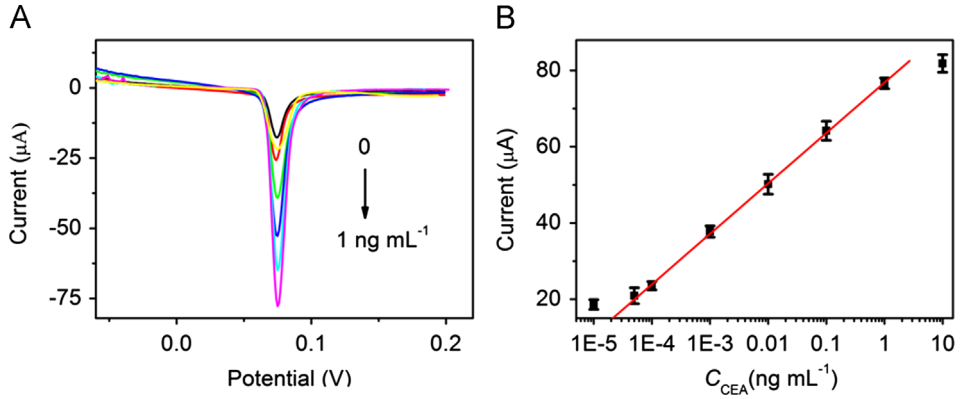

Fig. 4. (A) Stripping voltammetric responses at CEA concentrations of 0, 0.05, 0.1, 1.0, 10, 100 and 1000 pg mL^{-1}, and (B) calibration curve of the proposed method for CEA detection in 1.0 M KCl ($n=3$ for error bars).

promoted silver deposition amplification (Lin et al., 2012). In addition, this detection limit was also much lower than those obtained for CEA with AuNP-thionine-reduced graphene oxide-based sensor (Kong et al., 2011), DNA/$(ZMPs\text{-}HRP\text{-}anti\text{-}CEA)_n$ tag (Gan et al., 2011), and HRP-anti-CEA/AuNP-graphene oxide tag (Chen et al., 2012), and approached the detection limit of 3 fg mL^{-1} for CEA with AuNP-phenylenediamine-based sensor (Sun and Ma, 2012). High sensitivity and low limit of detection could improve the detection precision and be suitable for detecting low-abundance biomarkers in serum samples, indicating great promise for practical application.

Both the intra-assay and inter-assay precisions of the immunosensors were examined with 0.1 ng mL^{-1} CEA for five times. The relative standard deviations (RSD) were 6.2% and 7.6%, respectively, showing the good precision and acceptable fabrication reproducibility. In addition, when the immunosensor was stored in dry at 4 °C, over 92% of the initial response was remained after a storage period of 15 days. These results indicated that the immunosensor had acceptable reliability and stability, and was suitable for the clinical detection of protein markers.

3.5. *Application in detection of serum tumor marker*

The analytical reliability and application potential of the proposed method was evaluated by comparing the assay results of clinical serum samples using the proposed immunosensor with the reference values obtained by commercial electrochemiluminescent tests. Due to the high sensitivity, serum samples were appropriately diluted with 0.02 M pH 7.4 PBS prior to assay. The results showed an acceptable agreement with relative errors less than 11.9% (Table S1), indicating acceptable accuracy of the proposed method for the detection of CEA in clinical samples.

4. Conclusions

An ultrasensitive electrochemical immunoassay method was developed with nanogold/mesoporous carbon foam-mediated silver enhancement. The Au/MCF could be conveniently synthesized by in situ growth of nanogold on carboxylated MCF and be easily labeled to the signal antibody. The high loading of nanogold on MCF caused a C–Au synergistic silver enhancement and hence greatly amplified the detection signal and improved the detection sensitivity. With the electrochemical stripping analysis of the deposited silver, the proposed method showed a wide detection range and an ultralow detection limit for CEA. Moreover, this method avoided the shortcoming of the enzyme-related immunoassay and the need of deoxygenation, thus provided a promising potential in clinical diagnosis, especially in point-of-care testing.

Acknowledgments

We gratefully acknowledge the National Basic Research Program (2010CB732400), the National Natural Science Foundation of China (21075055, 21135002, 21121091 and 21105046), PhD Fund for Young Teachers (20110091120012), the Leading Medical Talents Program from Department of Health of Jiangsu Province, and Natural Science Foundation of Jiangsu (BK2011552).

Appendix A. Supporting information

Supplementary data associated with this article can be found in the online version at http://dx.doi.org/10.1016/j.bios.2013.08.051.

References

Boo, H., Jeong, R.A., Park, S., Kim, K.S., An, K.H., Lee, Y.H., Han, J.H., Kim, H.C., Chung, T.D., 2005. Analytical Chemistry 78, 617–620.

Chen, H.F., Tang, D.P., Zhang, B., Liu, B.Q., Cui, Y.L., Chen, G.N., 2012. Talanta 91, 95–102.

Darbha, G.K., Singh, A.K., Rai, U.S., Yu, E., Yu, H.T., Chandra Ray, P., 2008. Journal of the American Chemical Society 130, 8038–8043.

Datta, K.K.R., Reddy, B.V.S., Ariga, K., Vinu, A., 2010. Angewandte Chemie International Edition 49, 5961–5965.

Deng, Y.H., Cai, Y., Sun, Z.K., Gu, D., Wei, J., Li, W., Guo, X.H., Yang, J.P., Zhao, D.Y., 2010. Advanced Functional Materials 20, 3658–3665.

Dequaire, M., Degrand, C., Limoges, B., 2000. Analytical Chemistry 72, 5521–5528.

Du, D., Wang, L.M., Shao, Y.Y., Wang, J., Engelhard, M.H., Lin, Y.H., 2011. Analytical Chemistry 83, 746–752.

Gan, N., Jia, L.Y., Zheng, L., 2011. International Journal of Molecular Sciences 12, 7410–7423.

Ho, J.A., Chang, H.C., Shih, N.Y., Wu, L.C., Chang, Y.F., Chen, C.C., Chou, C., 2010. Analytical Chemistry 82, 5944–5950.

Katz, E., Willner, I., 2004. Angewandte Chemie International Edition 43, 6042–6108.

Kim, D., Daniel, W.L., Mirkin, C.A., 2009. Analytical Chemistry 81, 9183–9187.

Kong, F.Y., Xu, M.T., Xu, J.J., Chen, H.Y., 2011. Talanta 85, 2620–2625.

Lai, G.S., Wu, J., Ju, H.X., Yan, F., 2011. Advanced Functional Materials 21, 2938–2943.

Li, J., Tang, S., Lu, L., Zeng, H.C., 2007. Journal of the American Chemical Society 129, 9401–9409.

Lin, D.J., Wu, J., Wang, M., Yan, F., Ju, H.X., 2012. Analytical Chemistry 84, 3662–3668.

Lin, D.J, Wu, J., Ju, H.X, Yan, F., 2013. Biosensors and Bioelectronics 45, 195–200.

Liu, B.Q., Li, Q.F., Zhang, B., Cui, Y.L., Chen, H.F., Chen, G.N., Tang, D.P., 2011. Nanoscale 3, 2220–2226.

Lu, J.J, Liu, S.Q., Ge, S.G., Yan, M., Yu, J.H., Hu, X.T., 2012. Biosensors and Bioelectronics 33, 29–35.

Malhotra, R., Patel, V., Vaque, J.P., Gutkind, J.S., Rusling, J.F., 2010. Analytical Chemistry 82, 3118–3123.

Nie, H.G., Liu, L.S., Yu, R.Q., Jiang, J.H., 2009. Angewandte Chemie International Edition 48, 9862–9866.

Prieto, G., Meeldijk, J.D., de Jong, K.P., de Jongh, P.E., 2013. Journal of Catalysis 303, 31–40.

Qu, F.L., Lu, H.M., Yang, M.H., Deng, C.Y., 2011. Biosensors and Bioelectronics 26, 4810–4814.

Sidransky, D., 2002. Nature Reviews Cancer 2, 210–219.

Sun, X., Ma, Z., 2012. Biosensors and Bioelectronics 35, 470–474.

Tang, D.P., Hou, L., Niessner, R., Xu, M., Gao, Z.Q., Knopp, D., 2013. Biosensors and Bioelectronics 46, 37–43.

Tang, J., Tang, D., Li, Q.F., Su, B.L., Qiu, B., Chen, G.N., 2011. Analytica Chimica Acta 697, 16–22.

Tao, X.Y., Chen, X.R., Xia, Y., Huang, H., Gan, Y.Q., Wu, R., Chen, F., Zhang, W.K., 2013. Journal of Materials Chemistry A 1, 3295–3301.

Taton, T.A., Mirkin, C.A., Letsinger, R.L., 2000. Science 289, 1757–1760.

Ting, B.P., Zhang, J., Khan, M., Yang, Y.Y., Ying, J.Y., 2009. Chemical Communications, 6231–6233.

Walcarius, A., 2012. Trac-Trends in Analytical Chemistry 38, 79–97.

Wan, Y., Wang, Y., Wu, J.J., Zhang, D., 2011. Analytical Chemistry 83, 648–653.

Wang, J., Liu, G., Jan, M.R., 2004. Journal of the American Chemical Society 126, 3010–3011.

Wang, Y., Shao, Y.Y., Matson, D.W., Li, J.H., Lin, Y.H., 2010. ACS Nano 4, 1790–1798.

Wu, S., Ju, H.X., Liu, Y., 2007. Advanced Functional Materials 17, 585–592.

Wu, Y.F., Chen, C.L., Liu, S.Q., 2009. Analytical Chemistry 81, 1600–1607.

Wu, Y.F., Xue, P., Kang, Y.J., Hui, K.M., 2013. Analytical Chemistry 85, 3166–3173.

Wulfkuhle, J.D., Liotta, L.A., Petricoin, E.F., 2003. Nature Reviews Cancer 3, 267–275.

Zhou, M., Shang, L., Li, B.L., Huang, L.J., Dong, S.J., 2008. Biosensors and Bioelectronics 24, 442–447.

Zhuo, Y., Yuan, P.X., Yuan, R., Chai, Y.Q., Hong, C.L., 2009. Biomaterials 30, 2284–2290.